

FINAL REPORT  
U.S. Department of Energy

PHOTOOXIDATION OF ORGANIC WASTES USING SEMICONDUCTOR  
NANOCLUSTERS

Principal Investigator: Jess P. Wilcoxon  
Institution: Sandia National Laboratories  
Collaborators: J.E. Martin, T.R. Thurston, D.F. Kelley  
Institutions: Sandia National Laboratories, Colorado State University

Project Number: 55387  
Project Duration: 1/1/97 to 1/15/00

**Table of Contents**

1. Executive Summary.....	2
2. Research Objectives.....	3
3. Introduction.....	3
4. Methods.....	6
Synthesis.....	6
Purification/Processing.....	6
Catalyst Characterization.....	7
Catalyst Optical Properties.....	8
Photooxidation Reactor.....	8
5. Results.....	9
Photooxidation of an Alkyl Chloride.....	9
Phenol Destruction With Visible Light.....	11
MoS <sub>2</sub> Supported Catalysts for Phenol Photooxidation.....	12
PCP Photooxidation Kinetics.....	14
Effect of Incident Light Intensity.....	17
PCP Photooxidation using nanosize MoS <sub>2</sub> .....	19
6. Relevance, Impact and Technology Transfer.....	21
7. Project Productivity.....	21
8. Publications.....	21
Peer Reviewed.....	21
Submitted/Accepted.....	21
9. Interactions.....	22
Presentations.....	22
Collaborations.....	22
10. Patents.....	22
11. Future Work.....	22
12. Literature Cited.....	22

## Figures

1. Solar Irradiance and Catalyst Absorbance.....	4
2. Semiconductor Band-gap Potentials.....	6
3. Absorbance Properties of Catalysts.....	9
4. Absorbance Chromatogram of Alkyl Chloride and MoS <sub>2</sub> .....	10
5. Absorbance of MoS <sub>2</sub> before and after Reaction.....	10
6. Phenol Photooxidation vs. Irradiation Time.....	11
7. Phenol Photocatalysis using MoS <sub>2</sub> on TiO <sub>2</sub> .....	13
8. Absorbance Chromatogram for PCP using SnO <sub>2</sub> .....	16
9. PCP Concentration vs. Irradiation time for various catalysts.....	16
10. PCP Concentration vs. Irradiation time vs.intensity for TiO <sub>2</sub> .....	18
11. PCP Concentration vs. Irradiation time vs.intensity for SnO <sub>2</sub> .....	18
12. PCP Concentration vs. Irradiation time for various catalysts.....	19

## EXECUTIVE SUMMARY

Contamination of sediments and aqueous water systems by halogenated organic compounds presents a serious environmental threat due to their toxicity and resistance to biodegradation. These chemicals are widely employed as pesticides, insecticides, and wood preservatives and thus are ubiquitous in the environment of both industrialized and agrarian nations. Even chemicals which have been banned for years, like DDT and its analogs, still pose major environmental threats and in fact, constitute the basis of several EPA superfund sites. A subgroup of these chemicals, referred to as chlorinated aromatics, includes chlorinated benzenes, biphenyls (PCBs), pentachlorophenol (PCP), and insecticides such as DDT.

Microbial degradation and naturally occurring hydrolysis of these compounds is a very slow process (e.g. for 4-chlorophenol at 9 °C the half life is nearly 500 days). Some direct photodegradation also occurs, though the limited optical absorbance of chlorinated aromatics above 350 nm in wavelength makes this process painfully slow. Sometimes this direct photolysis can actually lead to more toxic products (e.g. direct photolysis of PCP has been reported to lead to octachlorodibenzo-p-dioxin, an even more toxic species than its precursor).<sup>3</sup>

It is clear that more effective methods of treatment of these chlorinated aromatics must be sought.<sup>1-4</sup> To this end, a few groups have been investigating photocatalytic oxidation of these compounds to form harmless CO<sub>2</sub> and HCl, a process referred to as total mineralization. The semiconductor catalyst of choice in these studies has been TiO<sub>2</sub>, a white, photostable, non-toxic powder, whose principal deficiency is an absorbance edge which starts at about 385 nm, allowing less than 3% utilization of the solar spectrum.

We demonstrated that in small nanosize clusters of MoS<sub>2</sub>, the electronic properties, such as the position of the conductance and valence bands, are size dependent. Using this novel property we were able to demonstrate for the first time visible light driven photooxidation of phenol and PCP, achieving complete mineralization. In fact, the performance of our best 3.0 nm MoS<sub>2</sub> photocatalyst, using only visible light (400 <  $\lambda$  < 700 nm), was superior to that of the best commercially available photocatalytic material, Degussa P-25 TiO<sub>2</sub> using the entire spectrum from 300 <  $\lambda$  < 700 nm.

Other program highlights include our ability to deposit nanosize MoS<sub>2</sub> on bulk powders of TiO<sub>2</sub> as well as using this hybrid photocatalyst with only visible light to photooxidize phenol to CO<sub>2</sub>. We showed there was a strong size dependence to the photocatalytic activity of MoS<sub>2</sub> and demonstrated by comparison to nanosize SnO<sub>2</sub> that this effect was not due to increased surface area, but rather the electronic changes that occur in semiconductor materials when the size is less than ~5 nm.

We showed that nanosize SnO<sub>2</sub> could also compete effectively with Degussa P-25 TiO<sub>2</sub> and studied the effect of the incident light intensity on this material on the photooxidation of PCP. This is the first time this inexpensive, non-toxic material has been shown to be effective for such an application.

Finally, we demonstrated that the use of certain cationic surfactants on the surface of the nanosize materials (and even ordinary bulk powder catalysts) could actually enhance the photocatalytic activity. Using such optimized nanosize materials we demonstrated the successful mineralization of a combination of three toxic chlorinated compounds (Phenol, PCP, and 4-Cl-Phenol) for the first time.

### **RESEARCH OBJECTIVES:**

It would be a major boon to have a visible light absorbing semiconductor catalytic material available, which is also photostable and non-toxic. Such a photocatalyst would make it possible to exploit sunlight as the sole energy source required for detoxification. To this end we have employed our expertise in nanocluster synthesis and processing to make and purify nanoparticles of MoS<sub>2</sub>. The band-gap and absorbance edges of these nanoparticles can be adjusted by particle size based upon the quantum confinement of the electron-hole pair. In a recent paper we demonstrated the use of these new photocatalysts to destroy phenol, and demonstrated a strong effect of size or band-gap on the rate of photo-oxidation.<sup>5</sup>

In this research we investigate the photooxidation kinetics and products formed for a standard material, Degussa P-25 TiO<sub>2</sub>, as compared to nanosize TiO<sub>2</sub>, SnO<sub>2</sub>, and MoS<sub>2</sub>. We examined the light intensity dependence for nanosize SnO<sub>2</sub> compared to TiO<sub>2</sub> (Degussa), and the effect of size on photooxidation kinetics for both SnO<sub>2</sub> and MoS<sub>2</sub>. We studied photooxidation in aqueous systems and, for the first time, a system consisting almost entirely of a polar organic, acetonitrile.

Our primary objective was to develop an entirely new class of material: nanosize semiconductors with visible bandgaps and to engineer these material's properties to allow us to photooxidize toxic organic compounds in water on a reasonable time scale (~8 hrs). A second objective was to study how certain material properties such as size, surface treatment, and material type affect the efficiency of the photocatalytic process as well as optimizing these features.

### **INTRODUCTION**

The electron-hole pairs generated by solar radiation in semiconducting materials can catalyze redox reactions that destroy organic chemicals, a process with obvious environmental remediation potential. A significant amount of research on semiconductor catalyzed photo-oxidation of organic chemicals has consequently been done during the past 15 years. Most studies have examined the photocatalytic activity of TiO<sub>2</sub>. This material has shown great promise, with many beneficial characteristics including; the ability to catalyze the destruction of a wide variety of organic chemicals, complete oxidation of organics to CO<sub>2</sub> and dilute mineral acids in many cases, lack of inherent toxicity, resistance to photodegradation and cheapness. In spite of all these propitious properties, TiO<sub>2</sub>-based photo-oxidation technology has still not been commercialized.

Two major disadvantages of  $\text{TiO}_2$ -based photo-oxidation technology are the lack of adequate fixed bed reactor designs and the large band gap of  $\text{TiO}_2$  ( $\sim 3.2$  eV). The former problem seems solvable in the near future, however, the latter problem is more difficult to circumvent. Figure 1 illustrates the band gap issue. This plot shows the spectral irradiance of the solar spectrum at the earth's surface as a function of photon wavelength, along with the band gap wavelength of some of the materials examined in this work. Only photons with wavelengths smaller than the band gap wavelength can excite electron-hole pairs. For bulk  $\text{TiO}_2$ , this wavelength is in the near UV region,  $\sim 390$  nm, which means that only a tiny fraction ( $\sim 3\%$ ) of the solar spectrum can be harvested. This deficiency was quickly recognized, and previous efforts to ameliorate this problem have involved coating the  $\text{TiO}_2$  with photosensitizers such as dyes. It is not clear that this approach will ultimately be commercially viable, since the dye molecules themselves can be photo-oxidized.

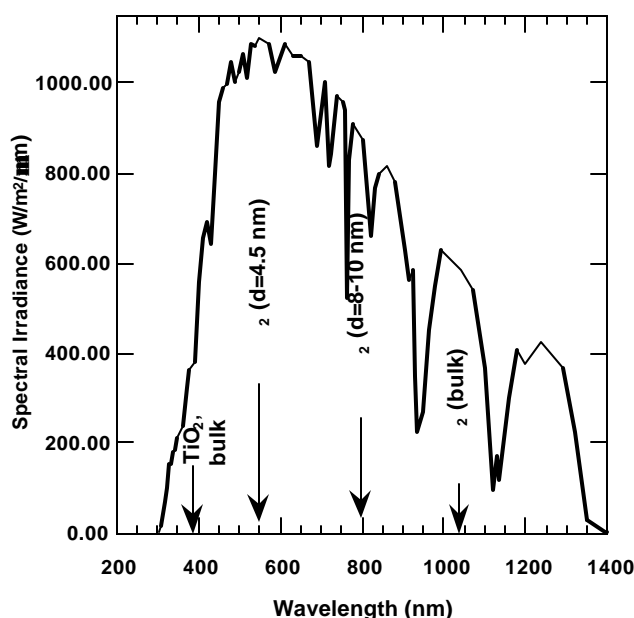


FIG. 1. Spectral irradiance of the solar radiation that reaches the earth's surface as a function of photon wavelength (AM1.5D). The dips in the spectrum arise from absorbance in the earth's atmosphere. The absorbance edge of various semiconductor compounds examined in this work are also shown.

In this work we explore the photocatalytic properties of a possible alternative to  $\text{TiO}_2$ , nanosize  $\text{MoS}_2$ . We chose to investigate this particular material for several reasons. Bulk  $\text{MoS}_2$ , has a anisotropic, layered, graphite-like structure consisting of S-Mo-S sandwiches held together by weak Van-der-Waals forces. The electronic states of the conduction and valence bands are both derived primarily from Mo 4d orbitals. Photoexcitation of electrons therefore should not significantly weaken bonds between the Mo and S atoms, which leads to enhanced photodegradation resistance. Indeed, previous researchers have shown that defect-free bulk  $\text{MoS}_2$  is remarkably photostable during photoelectrochemical oxidation of water. When photo-oxidation of bulk electrodes of  $\text{MoS}_2$  does occur, it happens at step defects in the semiconductor film where Mo edge site atoms are not protected by the inert basal planes of sulfur atoms. This results in dissolution of the lattice via oxidation of sulfur to

sulfate ions. However, this process is quite slow in this covalent material compared to ionic semiconductor electrodes like CdS.

The valence band of CdS, though thermodynamically stable compared to water oxidation, is kinetically unstable. The instability to photooxidation of the lattice is partially due to the ionic character of this semiconductor which means that the valence band is derived primarily from S 3p orbitals and the conduction band from Cd 5s orbitals. Not surprisingly, CdS readily photodegrades, releasing toxic cadmium ions upon illumination. Never-the-less, Gratzel has shown that for other photo-oxidation reactions such as H<sub>2</sub>S oxidation to elemental sulfur, the different kinetic pathway prevents photo-oxidation of the lattice. So, the issue of photostability in any semiconductor system is primarily kinetic, not thermodynamic as was recently pointed out by Tributsch in an excellent review article.

An advantage of MoS<sub>2</sub> compared to photostable, wide-gap metal oxides such as TiO<sub>2</sub> is that the band gap of MoS<sub>2</sub> is small enough to allow most of the solar spectrum to be harvested. As discussed below, only nanoscale MoS<sub>2</sub> clusters are photochemically active for  $\lambda > 400$  nm, and these materials can have their band gaps shifted from the bulk value by various amounts by quantum size effects.. For example, the bulk indirect absorbance edge of MoS<sub>2</sub> is ~1040 nm while a solution of 4.5 nm MoS<sub>2</sub> nanoclusters absorbs visible light starting at ~550 nm. Figure 1 illustrates this effect for some of the nanoclusters examined in this work. So, a large fraction of the solar spectrum can be harvested by these nanoscale semiconductors.

Quantum size effects that increase the band gap in nanoscale MoS<sub>2</sub> also shift the redox potentials of the conduction and valence bands in advantageous ways. We have recently estimated the size of this effect by studying the kinetics of electron transfer to bipyridine.<sup>6</sup> A potential energy shift is necessary for MoS<sub>2</sub> to function as a photo-oxidation catalyst. This issue is illustrated in figure 2, which shows the redox potentials of TiO<sub>2</sub> and MoS<sub>2</sub> (based upon the lowest energy indirect transition in both materials) of various sizes versus the normal hydrogen electrode potential (NHE). For TiO<sub>2</sub>, the oxidation process appears to be dependent on the formation of surface adsorbed hydroxyl radicals ( $\bullet$ OH) from adsorbed water by valence band holes, with a corresponding reduction of dissolved molecular oxygen by conduction band electrons (provided no other reducible species is present). At pH=7 solution, the production of  $\bullet$ OH radicals will occur if the semiconductor valence band potential is larger than +1.20-1.5 V. A possible mechanism for  $\bullet$ OH production is  $\text{Mo(IV)} \dots \text{H}_2\text{O} + \text{h}^+ = \text{Mo(IV)-OH} + \text{h}^+$ , which, for the analogous Ti(IV) system in TiO<sub>2</sub>, has a redox potential of  $1.5 \pm 0.3$  V vs NHE. This will occur at the abundant Mo edge sites of a nanocluster. Another possible source of  $\bullet$ OH production can occur by hole transfer from nanosize MoS<sub>2</sub> to bound H<sub>2</sub>O in the presence of O<sub>2</sub> to produce hydrogen peroxide. This has a redox potential of ~1.2 V vs. NHE.

It is easy to understand why only nanoscale MoS<sub>2</sub> will be catalytically active. As shown in figure 2, the oxidation potential of bulk MoS<sub>2</sub> is not sufficiently large to produce  $\bullet$ OH radicals. On the other hand, the same quantum size effects that increase the band gap in nanoscale MoS<sub>2</sub> will also shift the valence band enough to permit  $\bullet$ OH production. In addition, the shift of the reduction potential to more negative values should accelerate the transfer of electrons to dissolved oxygen to form chemical species that will also attack organic molecules.

A significant advantage of nanocluster semiconductor particles is that the surface trapping of electrons and holes before recombination may be more efficient in small particles. The photogenerated electron-hole pairs have a much shorter distance to travel to reach the surface in a small cluster. Once the electrons and holes have been trapped at the interface, they can then participate in redox reactions.

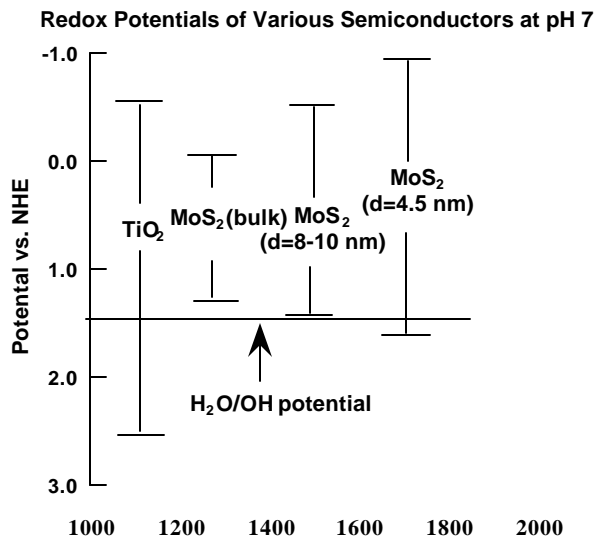


FIG. 2. Position of the conduction and valence band edges vs. normal hydrogen electrode (NHE) for bulk TiO<sub>2</sub> and MoS<sub>2</sub> of various sizes. If the valence band edge is more positive than +1.2-1.5 V, photogenerated holes can oxidize water and create hydroxyl radicals which can then oxidize dissolved organic chemicals.

Nanoparticles of the size of the MoS<sub>2</sub> in this work also scatter negligible amounts of light. Unlike slurries of bulk semiconductor powders which intensely multiply scatter all the incident light, light extinction in solutions of semiconductor nanoclusters occurs solely via absorbance. This may make understanding and modeling their photocatalytic behavior simpler.

## METHODS

### Synthesis

The MoS<sub>2</sub> nanoclusters were made with an inverse micelle technique. We briefly describe the synthesis here, more detailed descriptions are given elsewhere. Inverse micelles are formed when surfactant molecules are dispersed in a nonpolar (e.g., octane, oil) continuous medium. In such a solution, the hydrophilic ends of the surfactant molecules avoid the oil and form droplet-like cages whose sizes typically range from one to tens of nanometers. MoS<sub>2</sub> clusters are formed by first dissolving a molybdenum (IV) halide salt inside the cages and then combining this solution with another inverse micelle solution containing a sulfiding agent (e.g., metal sulfide or H<sub>2</sub>S). The synthesis is done in a dry box with catalytic oxygen and water removal to prevent degradation of the Mo (IV) salt precursor. Both oxygen and water levels were monitored and kept below 1 ppm during the reaction. The Mo:S ratio was chosen to be 1:2 or less. The cluster size is varied by using different sized micelle cages to encapsulate the Mo salt.

### Purification/Processing of the Nanocatalysts

The as-synthesized MoS<sub>2</sub> nanoclusters were purified by extraction from the non-polar solution in which they were prepared, octane into a water miscible but octane immiscible solvent, acetonitrile (ACN). The MoS<sub>2</sub> clusters in ACN were dried to a very small volume (e.g. ~0.5 ml) by centrifugal evaporation (~40x reduction in volume) using a Centrивap™ (Labconco Corp.) with a cold trap, and then these reduced volume samples were added to water to form the catalyst solution.

Removal of ions, excess surfactants, and isopropanol from the nanocluster solutions of MoS<sub>2</sub>, TiO<sub>2</sub>, and SnO<sub>2</sub> using the as-prepared solutions was achieved by dialysis using a 500 M.W. cut-off Spectra-Por™ (Spectrum Medical Industries, Inc.) dialysis membrane and dialysis against 1 liter of milli-Q water with one change over a 12-24 hour period. Some aggregation, as determined by DLS of the MoS<sub>2</sub> and TiO<sub>2</sub>, nanoclusters occurred under these conditions, but the catalytic activity improved substantially. The nanoclusters solutions were still visually transparent, stable without agitation, and non-turbid. All nanocluster catalyst solutions exhibited negligible light scattering in contrast to the control suspension of Degussa TiO<sub>2</sub> at a concentration of 0.1 mg/ml which was milky white, cloudy, and exhibited intense multiple scattering. We note that the concentration of TiO<sub>2</sub> used in the present studies was about 16-20 times less than that used in most previous work to try to minimize multiple scattering effects on the control catalyst. Even so, the intense multiple scattering characteristic of slurries of TiO<sub>2</sub> or CdS makes direct comparison of the quantum efficiency (Q.E.) of Degussa TiO<sub>2</sub> to the corresponding nanocluster solutions very difficult. Viable realistic approaches to address this issue have been discussed extensively in the literature.

### Catalyst Characterization

TEM and HRTEM were used to determine the nanocrystallinity of the materials, average cluster size, and polydispersity. The results were corroborated by use of DLS to measure the hydrodynamic diameter of the clusters in solution at the pH used for the photooxidation experiments. Except for nanosize TiO<sub>2</sub> this pH was ~4.0 (the typical pH of our deionized milli-Q™ water) and the solution was not buffered, nor purged with any gases. It was necessary to keep the pH of the nanosize TiO<sub>2</sub> solutions at pH~2.0 to prevent aggregation. In the case of MoS<sub>2</sub>, the clusters were so small that TEM gives a better measure of cluster size than DLS, but in the other cases, the sizes reported were obtained from DLS which gives a better ensemble averaged size than TEM.

SAD has been used to determine that, for the case of nanoclusters of MoS<sub>2</sub> clusters large enough to give good electron diffraction (i.e.  $d > 4.5$  nm), a crystal structure identical to bulk MoS<sub>2</sub> was observed. XRD from a  $d = 4.5$  nm MoS<sub>2</sub> solution dried to form a powder was compared to data from a commercial MoS<sub>2</sub> (99.7%, Alfa) powder obtained on the same instrument. Except for the broadening due to the small domain size, the structures are identical. Further details concerning the optical properties and physical characterization of MoS<sub>2</sub> are given elsewhere.<sup>7</sup>

X-ray Fluorescence (XRF) spectroscopy (Spectrace QuantX™ system) was used to determine the inorganic composition of the purified, processed nanocluster solutions as well as to obtain the absolute metal concentrations indicated in later figures. Using XRF analysis, it was also possible to determine approximately the metal to sulfur ratio despite the notoriously low (~40 ppm) XRF sensitivity to low Z elements like S, and to compare this to bulk powders of MoS<sub>2</sub>. It was found that the ratio of Mo:S in our nanoclusters was ~1:2.5 to 1:3 showing some excess sulfur on the nanocluster surface which could not be removed by our purification procedures.

### Catalyst Optical Properties

The optical absorbance properties of our nanocluster catalysts were determined using a Cary 2300 UV-visible-NIR spectrometer at the same concentrations used in the photooxidation studies. Slurries of Degussa TiO<sub>2</sub> in water were shaken and the spectrum rapidly obtained before powder settling occurred. The results of these absorbance measurements for nanosize TiO<sub>2</sub>, SnO<sub>2</sub>, MoS<sub>2</sub>, and the Degussa TiO<sub>2</sub> slurries are shown in figure 4. The strong multiple scattering of semi-opaque TiO<sub>2</sub> slurries even at 0.1 mg/ml in the 0.2 cm path length cell obscures the true band-edge absorbance of this material, which is clearly exhibited by the optically clear 20 nm diameter TiO<sub>2</sub> nanocluster solution. As can be observed in this figure, the TiO<sub>2</sub> slurry multiple scattering effectively enhances the absorbance probability of a photon in the relevant range of light output from our Xe arc lamp (300 to 400 nm) which corresponds to the actual TiO<sub>2</sub> absorbance (see the TiO<sub>2</sub>(d=20 nm) nanocluster absorbance curve). Light scattering is negligible for SnO<sub>2</sub>, MoS<sub>2</sub>, and TiO<sub>2</sub> nanocluster solutions and the absorbance curves of figure 3 represent pure absorbance for these solutions.

### Photooxidation Reactor

Our photooxidation reactor consists of a custom built (Ace Glassware Co.) cylindrical reactor with a flat glass base and an o-ring sealed quartz, Ace threaded™ window holder with an aperture larger (~3 cm) than our collimated Xe lamp output beam, (~1.5 cm). The reactor has a total volume of about 60 ml, and we use 40 ml of liquid in all our reactions. The reactor has an o-ring sealed, Ace threaded™, 45° side arm for liquid or gas phase sampling through a septa. In all the studies to be described we simply removed the o-ring plug and sampled 0.6 ml of the sample at various irradiation times for analysis. This aliquot was filtered using an Hewlett-Packard HPLC filter (0.45 micron, cellulose) to remove suspended catalysts into a standard 2 ml crimp-top HP HPLC vial for either HPLC or GC/MS analysis. We tested to make sure no PCP was being adsorbed onto the filter. This filter allowed the nanosize catalysts to pass through, and so we could simultaneously do HPLC analysis of the MoS<sub>2</sub> nanocluster catalysts.

We used a commercial 400 Watt Xe-arc lamp from Oriel . The output of this lamp is very close to that of the solar spectrum when combined with the 700 nm short-pass filter used. Overhead illumination of the cylindrical reactor is very advantageous since the flat bottom geometry of our cell allows rapid magnetic stirring of the catalyst solution - a vital aspect affecting the photooxidation rate of the powder slurries used as control catalysts. This stirring is unimportant for the nanosize catalysts, but for consistency we maintained the same rate for these catalysts too. In order to study only visible light photooxidation a 400 nm long-pass filter was also used to limit the incident irradiation wavelength,  $\lambda$  to  $400 \text{ nm} < \lambda < 700 \text{ nm}$ . The lamp light output is monitored continuously by a Newport research (Newport Corp., Model 835) power meter with an IEEE-488 interface to a MacIntosh IICI computer, to track total irradiation time and any power variations. The incident power was measured using the 1 cm<sup>2</sup> size calibrated photodiode probe from Newport research Corp. Neutral density filters on suprasil quartz substrates (Oriel Corp.) were used to attenuate the incident light by known amounts.

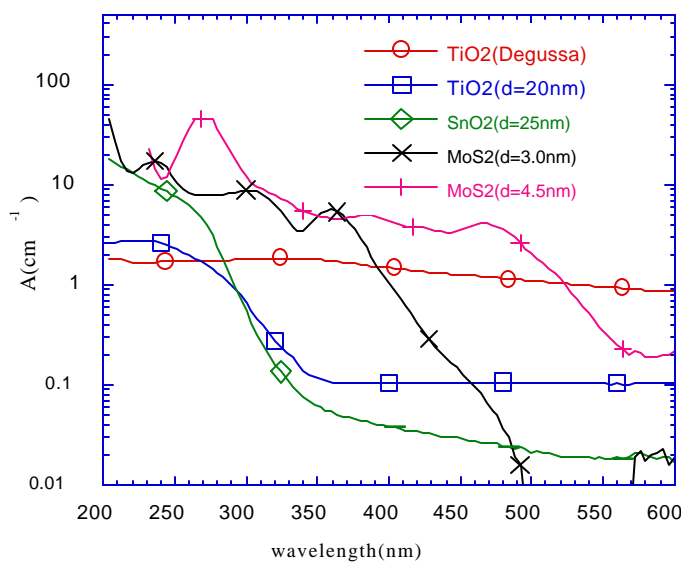


Fig. 3. UV-Visible absorbance spectra of nanocatalysts and control bulk powder (Degussa P-25, TiO<sub>2</sub>) are shown. All concentrations were 0.1 mg/ml.

## RESULTS

### Photooxidation of an Alkyl Chloride With Visible Light

We first demonstrated electron and hole transfer from nanosize MoS<sub>2</sub> using visible light and a sacrificial electron acceptor. In order to oxidize organic alkyl chlorides using visible light we needed to add an agent, e.g. bypyridine, (bpy) which could accept an electron and be reduced. In later reactions to be described we show that the role of sacrificial electron acceptor played by the bpy is not necessary. Using liquid chromatography analysis we have demonstrated that bypyridine binds strongly to nanosize MoS<sub>2</sub> and acts like an electron transfer relay to effect charge separation. The hole left behind on MoS<sub>2</sub> is then used to oxidize the organic impurities. In its reduced form bypyridine complexes to the oxidized organic impurity and precipitates out of solution. We studied the chemistry of this process by high pressure liquid chromatography which separates each of the chemicals in the solution from the MoS<sub>2</sub> photocatalyst. The results of this experiment are shown in figure 4. The initially present organic impurity peak at  $t \sim 5.2$  minutes (an organic chloride) is destroyed as more bypyridine is added until it cannot be detected. However, the amount of nanosize MoS<sub>2</sub> remains unchanged, as measured by the area under the MoS<sub>2</sub> elution peak. Another, broader, organic peak observed in this figure at  $t \sim 4.7$  minutes also is destroyed by the MoS<sub>2</sub> as additional bpy is added, and at higher levels of bpy (not shown), is completely oxidized and precipitates out of solution as well. A white precipitate forms which can be removed from the solvent.

Studying the spectral properties of the MoS<sub>2</sub> before and after the reaction shows it has not changed in size, concentration, or photoproperties. The structured absorbance spectrum of the MoS<sub>2</sub> photocatalyst is shown in figure 5. Remarkably, the above photoredox reaction occurs rapidly (e.g. <1 minute) under ordinary room light (laboratory illumination) using these 3 nm nanoclusters which begin absorbing light at  $\sim 450$  nm. For larger, 4.5 nm MoS<sub>2</sub> with a narrower band gap which begin absorbing light near 550 nm, the reaction is significantly slower and less complete under room illumination. We

attribute this to the narrower bandgap and correspondingly lower reduction potential of these larger nanoclusters which provides less of a driving force for the electron transfer to bpy. For these larger clusters, which absorb more visible light, a stronger lamp source may be required to achieve complete photooxidation.

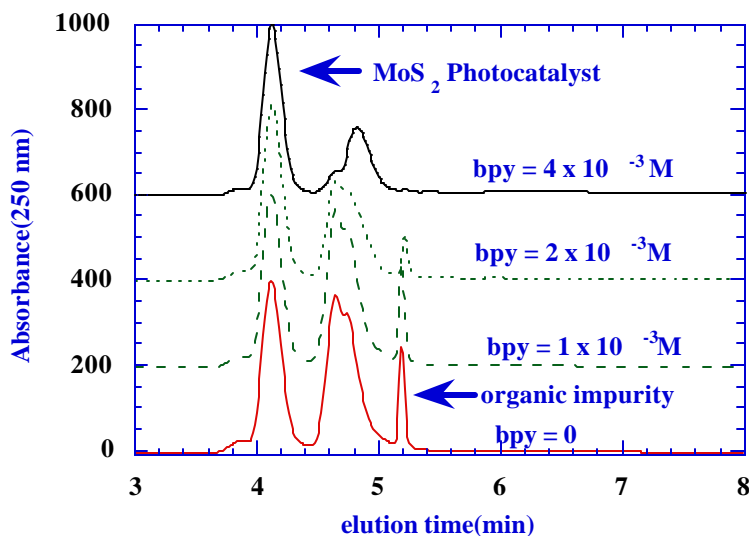


Figure 4. Plot of optical absorbance at 250 nm (a measure of the organic concentration) vs. elution time for impurity chemicals and MoS<sub>2</sub> nanoclusters. The organic impurities shown were photooxidized by the MoS<sub>2</sub> nanoclusters which have bipyridine (bpy) added to them. A new complex of the reduced bipyridine and oxidized organics is formed (see new elution peak at the upper trace). Due to its limited solubility, it precipitates and is removed from the solution.

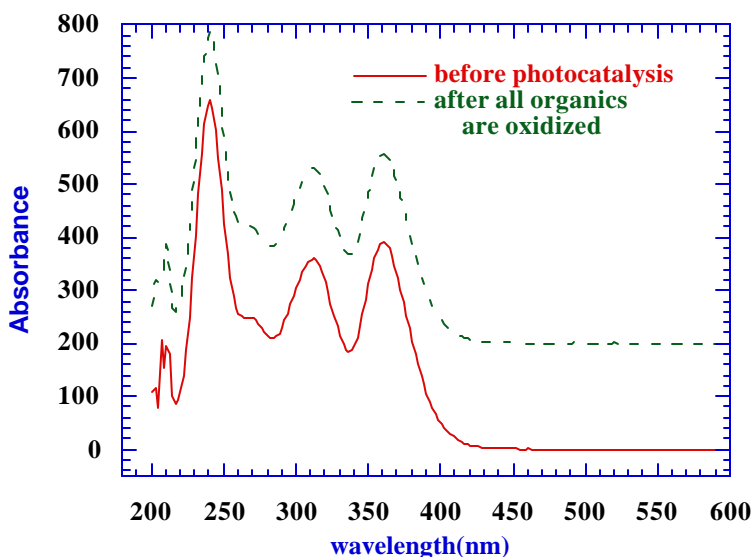


Figure 5. Plot of optical absorbance vs. wavelength for nanosize MoS<sub>2</sub> before and after photooxidation and precipitation of organic contaminants. No changes in either size or structure of the MoS<sub>2</sub> was observed. (The dashed curve has been shifted vertically for clarity).

### Phenol Destruction With Visible Light

One of our primary reasons for examining  $\text{MoS}_2$  nanoclusters was to try to find a nanoscale photocatalyst that is active when illuminated by visible radiation. In this regard, we were successful. Chromatographic results show the attempted photo-oxidation of phenol with visible radiation by equal concentrations of  $\text{MoS}_2$ (d=8-10 nm),  $\text{MoS}_2$ (d=4.5nm), and Degussa P25  $\text{TiO}_2$ . The illumination setup, as described above, used a 400 watt xenon arc lamp along with a 455 nm long-pass filter. In each case, the catalyst was mixed into ~40 ml  $\text{H}_2\text{O}$  and illuminated with 365 nm radiation over night. 4 ml of 200 mg/l phenol solution and enough  $\text{H}_2\text{O}$  to bring the solution up to 40 ml were then added, and after stirring for ~30 minutes in the dark, illumination with the arc lamp/455 nm filter was initiated. The phenol concentration as a function of time was monitored using HPLC.

For these reactions in which the nanosize  $\text{MoS}_2$  is fully dispersed, it is possible to detect an elution peak at earlier times (not shown) which was identified by its absorbance spectrum to be nanocluster  $\text{MoS}_2$ . The area of this peak and its complete absorbance spectrum for the surfactant-stabilized, d=4.5 nm  $\text{MoS}_2$  nanoclusters did not decrease during experiments with either visible illumination or 365 nm light, indicating this sample is acting as a true photocatalyst and it is not being photooxidized.

In figure 6, we show the phenol concentration as a function of time as determined from chromatograms such as those shown in figures 4. Under visible illumination there is a steady decline in the phenol concentration with  $\text{MoS}_2$ (d=4.5 nm) nanoclusters, a reduction in free phenol concentration at  $t=0$  due to adsorption to the bare  $\text{MoS}_2$ (d=8-10 nm) nanoclusters, and no phenol destruction with Degussa P25  $\text{TiO}_2$ . We were able to add additional phenol to the  $\text{MoS}_2$ (d=4.5 nm) nanocluster sample after most of the phenol was destroyed and reproduce the kinetics shown in figure 6 to within the error bar indicated on this figure.

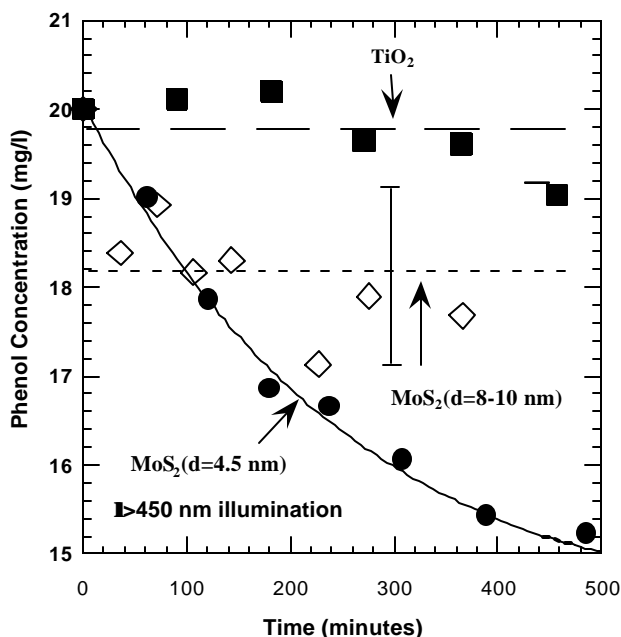


Fig. 6. Visible light driven phenol oxidation as a function of irradiance time as determined from HPLC chromatograms. The  $\text{MoS}_2$ (d=4.5 nm) nanoclusters catalyze phenol destruction with visible light, while the  $\text{MoS}_2$ (d=8-10 nm) nanoclusters initially adsorb phenol but fail to photooxidize it. Degussa P25

TiO<sub>2</sub>, which doesn't absorb visible light, shows no activity as expected. The lines are guides to the eye. The bar is the reproducibility of the HPLC measurements for independent runs.

Two control experiments were also performed. In the first, a 20 mg/l phenol solution was illuminated with the  $\lambda > 450$  nm set up and no catalyst. In the second, a MoS<sub>2</sub>(d=4.5 nm) nanocluster solution plus phenol solution was prepared but not illuminated. For each control experiment, no decline in the phenol concentration was observed. Thus, oxidation of the phenol is due to the presence of both MoS<sub>2</sub> catalyst and  $\lambda > 450$  nm radiation.

Figure 6 is the main result of this work. MoS<sub>2</sub> nanoclusters, if sufficiently small, photocatalyze the destruction of a difficult-to-oxidize compound with visible light. The lack of catalytic activity for the MoS<sub>2</sub>(d=8-10 nm) solution suggests that its valence band potential has not been shifted to positive enough values to produce hydroxyl radicals that can oxidize phenol. This observation is similar to experiments we have reported on photoreductive electron transfer from nanosize MoS<sub>2</sub> to bipyridine and tetramethyl substituted bipyridine. Nanocluster size played a critical role in the rate of electron transfer with the smallest clusters giving the fastest rates.

### MoS<sub>2</sub> Supported Catalysts for Phenol Photooxidation

Catalytic materials are often times deposited onto support materials. This is done not only to prevent the catalyst from agglomerating, but often because reaction rates can be synergistically increased through interactions between the catalyst and support material. This strategy can be applied to semiconductor photocatalysts and, for MoS<sub>2</sub> nanoclusters, deposition on a support material may increase chemical photostability as well. Also, by combining two different semiconductor photocatalysts we can take advantage of the possibility of electron or hole transfer between the semiconductor catalysts, which could then lead to enhanced electron-hole lifetimes, and faster redox reaction rates. The latter possibility was first demonstrated in 1984 by Serpone *et al.*<sup>2</sup>

A series of experiments where MoS<sub>2</sub>(d=8-10 nm) nanoclusters were deposited onto TiO<sub>2</sub>, SnO<sub>2</sub>, WO<sub>3</sub>, and ZnO were performed. The deposition method was remarkably simple. Powdered support material was mixed into a solution of MoS<sub>2</sub> nanoclusters and then centrifuged with a vacuum applied. The solution slowly evaporated leaving nanoclusters deposited onto the support material. No heating or other treatments were performed, so further future improvements of contact interactions between the nanoclusters and semiconductor support material is possible. With this method it is not clear how uniform a dispersion can be obtained on the powder. In all cases, between 0 and 6 weight percent MoS<sub>2</sub> nanoclusters were deposited onto the support. The reaction rate for destruction of 20 mg/l phenol was then measured with a total (MoS<sub>2</sub> + support) catalyst density of 2 gm/l.

Figure 7 compares phenol destruction rates for three different loadings of MoS<sub>2</sub>(d=8-10 nm) on Degussa P25 TiO<sub>2</sub>. The 2.5 weight percent loaded sample destroyed the phenol faster than the unloaded sample, while the 5 weight percent loaded sample was slower. The data in figure 7 show that the initial destruction rate is a good predictor of the relative phenol concentration at all subsequent times. We therefore shall use the initial destruction rate to summarize relative catalytic activities. To do this, we fit data such as that shown in figure 7 to the phenomenological form

$$C = \frac{a + bt}{1 + ct}$$

where  $C$  is the phenol concentration,  $t$  the time, and  $a$ ,  $b$ , and  $c$  fitting parameters. From such fits, a rough estimate of the initial destruction rate can be found.

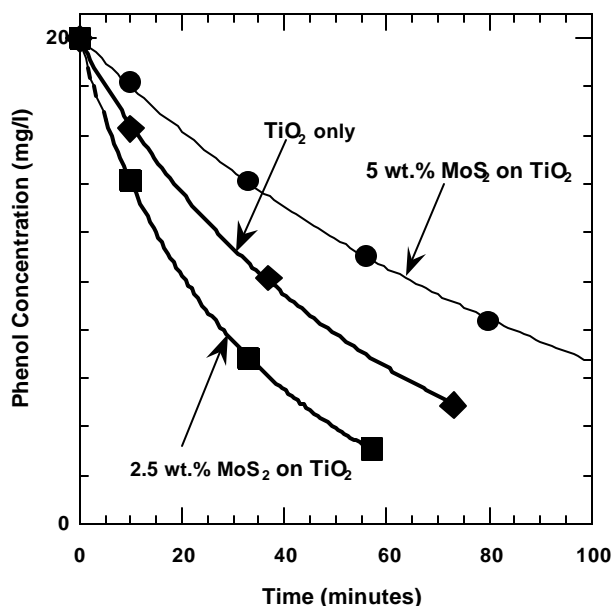


Fig. 7. Phenol concentration as a function of time as determined from HPLC chromatograms for Degussa TiO<sub>2</sub> loaded with 0, 2.5, and 5.1 weight percent MoS<sub>2</sub>(d=8-10 nm) nanoclusters. The radiation wavelength for this set of experiments was 365 nm.

The initial destruction rate as a function of MoS<sub>2</sub>(d=8-10nm) loading increases with wt% MoS<sub>2</sub> up to a factor of ~2 when the amount deposited is ~2.5 weight percent, and it then decreases with further loading. Conversely, in the absence of TiO<sub>2</sub> powder (i.e. dispersed MoS<sub>2</sub> nanoclusters alone at 0.05 gm/l) the phenol destruction rate is much smaller. These observations suggest that the nanosize MoS<sub>2</sub> and TiO<sub>2</sub> support are working in a cooperative manner to enhance the electron or hole transfer rate. Similar deposition experiments on other bulk metal oxide powders such as SnO<sub>2</sub>, WO<sub>3</sub>, or ZnO led to no enhancement in activity over the metal oxide by itself. These powders and other TiO<sub>2</sub> powders are all less active for phenol oxidation under identical reaction conditions than Degussa, P-25 TiO<sub>2</sub>.

The decrease in the initial reaction rate for loadings greater than 2.5 weight percent is somewhat puzzling. However, similar effects are often observed in traditional thermally activated metal catalysts deposited on metal oxide supports such as alumina, where the optimal metal loading often lies between 1 and 5 wt%. The belief, in this case, is that excessive metal loading reduces the state of dispersion of the metal (i.e., the available catalytically active surface area), via agglomeration processes during the *in situ* catalyst synthesis. However, since our supported semiconductor photocatalysts are synthesized in quite a different manner than traditional metal/metal oxide catalyst, a reduced state of dispersion may not be the best explanation in the present case. There may be two competing processes occurring when nanocluster MoS<sub>2</sub> is loaded onto TiO<sub>2</sub>, one which enhances phenol destruction and another which impedes it. A possible scenario which would rationalize our observations is that a small amount of deposited MoS<sub>2</sub> enhances phenol destruction through electron or hole transfer processes, but that excess amounts of MoS<sub>2</sub> impede phenol destruction by blocking important phenol binding sites on the TiO<sub>2</sub> surface.

### PCP Photooxidation Kinetics

To study the rate of photooxidation of PCP we used an HP 1050 High Pressure Liquid Chromatography (HPLC) system equipped with a photodiode array (PDA), a refractive index (RI), and a fluorescence (FL) detector(s). Unfortunately, the latter detector, though the ultimate in sensitivity for non-chlorinated aromatics like phenol, is nearly useless for PCP detection due to the quenching of the fluorescence by the chlorines on the aromatic ring of PCP. Never-the-less, we excited at 250 nm and detected fluorescence at 320 nm using this detector to detect any non-chlorinated aromatic by-products at the ppb level that might be formed during the photo-oxidation process. The entire spectrum from 200 nm (the solvent cut-off) to 600 nm is available at each time point in the elution peak chromatogram, but for quantitation purposes we chose to monitor at the three broad main features in the PCP spectrum, 325 nm, 250 nm, and 215 nm. The latter wavelength gives the most sensitivity, while the former two can be used to avoid any detector saturation effects at high PCP concentrations and to check for consistency. Stock solutions of 10, 1, and 0.1 ppm PCP in milli-Q™ (Millicore Corp.) water were prepared and a linear detector response over this concentration range was verified. A minimum sensitivity of about 0.02 ppm was determined for absorbance at 215 nm. This is significantly better sensitivity than we could achieve using our HP 5890/5972 GC/MS even using selective ion monitoring.

Obtaining acceptable peak elution symmetry and retention time stability from a highly chlorinated aromatic like PCP is a very challenging chromatography problem. We found that using an HP analytical ODS200 column (reverse phase c18 terminated silica, 200 mm (length) by 4.6 mm (diameter) with 5 mm particle packing and 120 Å pores) and running a 60:40 or 70:30 Methanol (MeOH):H<sub>2</sub>O mobile phase mixture gave the best elution profiles with good retention time stability over many runs. Various composition gradients of this mixture to 100% MeOH were also used to improve the separation if multiple organics were present. Using this solvent mixture it was also possible to detect the nanoclusters of MoS<sub>2</sub>, but we found that acetonitrile (ACN) gave more reproducibility for the nanocluster peak shape and elution time so a 60:40 ACN:H<sub>2</sub>O to 100% ACN was used in the MoS<sub>2</sub> nanocatalyst studies. This condition separates the nanoclusters, any surfactant, and PCP completely. We tried to use an independent column of the same type for the studies involving nanoclusters since some adsorption of the nanoclusters onto the column over many injections was found to alter the chromatographic elution behavior (i.e. peak shape, retention time) of the PCP, though not its quantitation (i.e. peak area). In all of our studies we inject 50 ml of the 600 ml sample taken at a given time point in the irradiation, and analyze the area under the elution peak at the three monitoring wavelengths, taking the average as the concentration of PCP at that point in time.

Generally, because of the low concentrations and limited solubility of PCP in water (~20 ppm), it is not possible to use gas chromatography/mass spectroscopy (GC/MS) to directly identify unknown photooxidation byproducts observed in HPLC using ion fragmentation patterns in MS, so we purchased several putative photooxidation intermediate candidates like tetrachlorocatechol from Aldrich chemicals and ran HPLC on these chemicals under identical chromatography conditions as used in the PCP photooxidation experiments. This allowed us to identify any possible intermediates via retention time alone. We also had the luxury of the complete absorbance spectrum of each elution peak to identify whether a compound observed was aromatic or not. Never-the-less, we were not able to identify all intermediates positively and we never observed tetrachlorocatechol, a logical intermediate to be formed by OH radical attack on a Cl on the PCP ring. However, our inability to identify most intermediates was not a major problem as all these compounds were eventually completely mineralized themselves.

Based upon the rate of appearance of these minor peaks compared to the rate of disappearance of the PCP peak, it was clear that these photooxidized compounds were not true intermediates on the pathway to complete mineralization, but rather, minor alternative photooxidation paths.

At the conclusion of several of the photooxidation reactions that were run long enough to achieve >99% disappearance of the PCP elution peak, we used a Cl<sup>-</sup> selective electrode to determine [Cl]. We were able to verify that the expected amount of free chloride was generated as calculated from the initial concentration of 10 ppm PCP, so complete detoxification was accomplished with the best nanosize photocatalysts using only visible illumination as well as with nanosize SnO<sub>2</sub> and Degussa TiO<sub>2</sub> using full (UV + visible) lamp illumination. Because of the small reactor volume and large Cl electrode size, it was not possible to follow the [Cl] *in situ*.

Using HPLC analysis we showed that the product intermediates in the photooxidation of PCP depend on whether a photocatalyst is used and also on the material type of the catalyst. Nanosize SnO<sub>2</sub>, for example, gave different products than powders of Degussa TiO<sub>2</sub> or nanosize MoS<sub>2</sub>.

Our photocatalytic oxidation results using nanosize SnO<sub>2</sub> are shown in figure 8 (bulk SnO<sub>2</sub> is nearly inactive for PCP photocatalysis). Here we observe breakdown products more similar to that of the direct photolysis results, but with accelerated kinetics. No peak at t=7.6 minutes corresponding to TiO<sub>2</sub> photocatalysis results is observed.

Nanosize SnO<sub>2</sub> has not been studied previously so these results cannot be compared directly to previous experiments. However, the rate of disappearance is comparable to that observed from Degussa TiO<sub>2</sub>. Since SnO<sub>2</sub> is cheaper than TiO<sub>2</sub>, but is ineffective as a bulk photocatalyst, these results are encouraging as they provide evidence that a robust metal oxide material in nanosize form can be competitive with Degussa TiO<sub>2</sub> slurries.

By integrating the areas observed in figure 8 and similar data collected for the other nanocluster catalysts studied, one can obtain the kinetics behavior shown in figure 9. There are obviously dramatically different rates of photooxidation of PCP for these various metal oxides. As has been found by many others, Degussa P-25 has remarkable catalytic activity compared to nanosize TiO<sub>2</sub> (d=20 nm). Two additional things can be immediately noted from this figure. The first is that the photooxidation kinetics of TiO<sub>2</sub> powder is non-exponential, while both nanosized SnO<sub>2</sub> solutions, the TiO<sub>2</sub> nanocluster solution, and the direct photolysis kinetics are nearly exponential. Secondly, though initially Degussa TiO<sub>2</sub> is more active than the SnO<sub>2</sub> nanoclusters, they all reach >99% complete mineralization in ~8 hrs.

In previous work by Mills et. al.,<sup>3</sup> the kinetics of photooxidation using Degussa P-25 TiO<sub>2</sub> at 0.2 mg/ml was observed to be 0<sup>th</sup> order in [PCP] for [PCP]>0.6 ppm. In contrast, Barbeni et al. showed first order behavior and an exponential decrease in [PCP] with irradiation time. Our results for both direct photolysis, and to a lesser extent photocatalysis using Degussa TiO<sub>2</sub> and nanosize TiO<sub>2</sub> and SnO<sub>2</sub>, also show an exponential decrease with time. However, the higher concentrations of TiO<sub>2</sub> used by previous workers, and the resulting stronger multiple scattering, may make previous determinations of the true kinetics ambiguous, as we show in our light intensity studies.

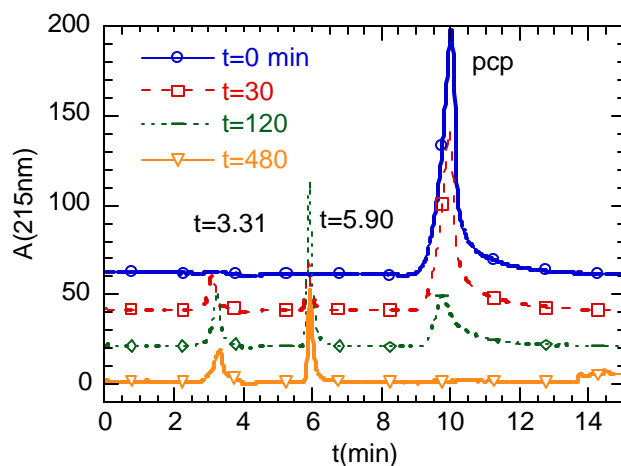


Fig. 8. Catalytic photooxidation of PCP in water containing 0.1 mg/ml  $d= 28$  nm,  $\text{SnO}_2$  is followed by the absorbance monitored by a PDA whose absorbance at 215 nm,  $A(215 \text{ nm})$  is plotted vs. elution time,  $t$ . Note the absence of the  $t=7.6$  byproduct found in  $\text{TiO}_2$  photooxidation and the formation of the by-products observed in direct photolysis at  $t=5.90$  and  $t=3.31$  minutes.

The apparently faster rate of photooxidation using Degussa P25  $\text{TiO}_2$  compared to the other materials is partly due to its intense multiple scattering of light which serves to confine the incident photons more effectively in the reactor. In other words, its *effective* absorbance cross-section is larger. The other nanosize photocatalyst solutions, being transparent, are somewhat light intensity limited at the 0.1 mg/ml or less nanocatalyst concentrations employed in these studies. This effect is illustrated most easily by comparison of the light intensity dependence of Degussa  $\text{TiO}_2$  vs. nanosize  $\text{SnO}_2$  as we do in the next section.

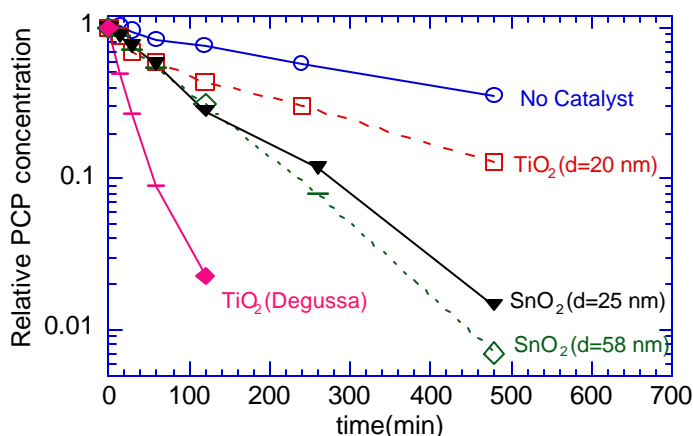


Fig. 9. Normalized PCP concentration vs. irradiation time using a 400 W Xe arc lamp with  $300 \text{ nm} < \lambda < 700 \text{ nm}$  irradiation. Initial PCP concentration was 10 ppm in all cases, and the incident light intensity was  $250 \text{ mW/cm}^2$ .

It appears from Figure 9 as if the larger sized,  $d=58$  nm  $\text{SnO}_2$  nanoclusters are slightly more effective for photo-oxidation of the PCP than the smaller  $d=25$  nm  $\text{SnO}_2$  nanoclusters, both at 0.1 mg/ml concentration. However, this inference is probably incorrect. We have run the PCP photooxidation reaction with the incident intensity reduced 10 fold in this case to see if photons are the "limiting reagent" in the nanocatalyst case but not in the  $\text{TiO}_2$  slurry suspension case.. In the latter case, the intense multiple scattering effectively increases the light path of the incident photons, and thus their absorbance probability, and so there are many more photons available than are needed for the reaction at the full lamp light intensity,  $250 \text{ mW/cm}^2$ . Thus, even when the photon intensity is reduced by an order of magnitude the slurry reaction doesn't slow proportionally, and the reaction kinetics are clearly not exponential under either of these conditions. However, under these irradiation conditions the nanocluster solutions are "starved" for photons and the reaction kinetics slow down in a proportional fashion as well as not exhibiting an exponential decrease in [PCP] with time.

We observe that there is no difference in photocatalytic oxidation activity for the two sizes of  $\text{SnO}_2$  nanoclusters under these lower light level conditions. From this observation we can conclude that an increase in specific surface area alone is not enough to accelerate the kinetics for nanoclusters in this colloidal size range. This observation contrasts markedly from that described below for smaller nanoclusters of  $\text{MoS}_2$ , where a very strong size dependence is observed due to quantum confinement effects.

*Effect of Incident Light Intensity On PCP Photooxidation Kinetics.* Because of the strong light dependence demonstrated in figure 9, we undertook a systematic investigation of the incident light intensity dependence of nanosize  $\text{SnO}_2$  compared to Degussa  $\text{TiO}_2$  powder slurries. We did not attempt to make a similar comparison in the case of nanosize  $\text{MoS}_2$  because of the significant difference in the absorbance edges of  $\text{TiO}_2$  and nanosize  $\text{MoS}_2$ .

Figure 10 shows the change in photooxidation rate of PCP using a slurry of 0.1 mg/ml Degussa  $\text{TiO}_2$  over a range of incident intensities of  $I_0 = 250 \text{ mW/cm}^2$  (no light attenuation) to  $I = 0.01 I_0$ . We were initially surprised by the very weak dependence of the kinetics on the incident intensity in the range  $0.1 I_0 < I < I_0$ . Apparently, due to extreme confinement of the light in the reactor due to multiple scattering from the slurry suspension, there are more than enough photons available so the reaction acts as if it is nearly zero order in the light intensity. Note that only when the light intensity is reduced by about a factor of 100-fold does the kinetics of PCP photooxidation become exponential, as is the case with all the nanosize photocatalysts investigated. Therefore, one should really be comparing the PCP photooxidation kinetics for nanosize  $\text{TiO}_2$  and  $\text{SnO}_2$  to slurries of  $\text{TiO}_2$  in this light intensity regime. Unfortunately, this intensity is at least 2 orders of magnitude lower than has been previously investigated using Degussa  $\text{TiO}_2$  and any organic.

Contrast the behavior shown in figure 10 by the slurry suspension of  $\text{TiO}_2$  to that exhibited by a nanocluster solution of  $\text{SnO}_2$  using the same reactor geometry and irradiation conditions. The results of this experiment are shown in figure 11. The same exponential PCP oxidation kinetics were observed for the nanosize  $\text{TiO}_2(d=20 \text{ nm})$ ,  $\text{SnO}_2(d=25 \text{ nm})$ ,  $\text{SnO}_2(d=58 \text{ nm})$ , and  $\text{MoS}_2(d=4.5 \text{ nm})$ . For each of the non-scattering nanocluster solutions we observe a rate that is roughly proportional to the incident light intensity, and the PCP oxidation kinetics appears exponential (i.e. first order in [PCP]) over the entire light intensity range investigated.

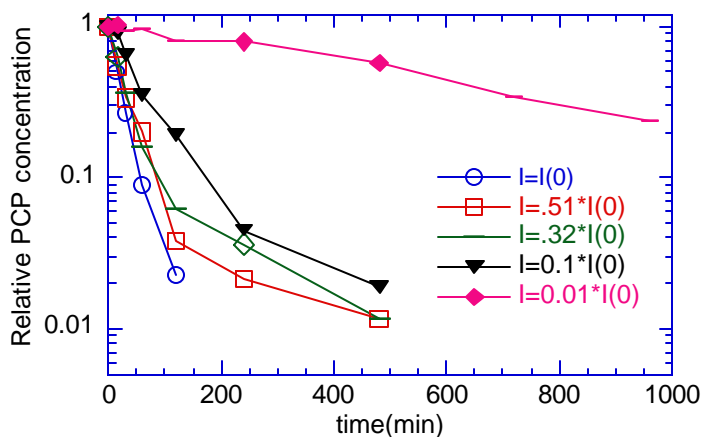


Fig. 10. Relative PCP concentration (all initial concentrations were 10 ppm in water) vs. irradiation time using a 400 W Xe arc lamp with the  $300 \text{ nm} < \lambda < 700 \text{ nm}$  pass filters and measured incident intensity of  $I_0 = 250 \text{ mW/cm}^2$  using Degussa P25  $\text{TiO}_2$  at 0.1 mg/ml.

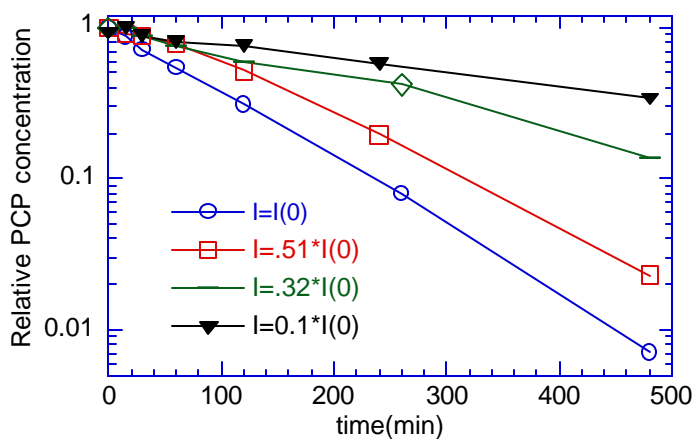


Fig. 11. Relative PCP concentration (all initial concentrations were 10 ppm in water) vs. irradiation time using a 400 W Xe arc lamp with the  $300 \text{ nm} < \lambda < 700 \text{ nm}$  pass filters and a measured incident intensity of  $I_0 = 250 \text{ mW/cm}^2$ , using nanosize,  $d = 26 \text{ nm}$   $\text{SnO}_2$  at 0.1 mg/ml.

We demonstrated a poisoning effect upon addition of a simple salt, NaCl, to slurries of  $\text{TiO}_2$ . More surprisingly, we observed that certain cationic surfactants actually enhance the activity of  $\text{TiO}_2$  slurries and the degree of enhancement depended on the counterion, Cl or Br. Furthermore, HPLC showed that these cationic surfactants were not photooxidized.

We made the first studies of PCP photooxidation using slurries of  $\text{TiO}_2$  and nanosize  $\text{SnO}_2$  in a polar organic solvent, ACN containing 1%  $\text{H}_2\text{O}$ . Surprisingly, we found significant, though reduced, photocatalytic activity for both types of catalysts, compared to pure  $\text{H}_2\text{O}$  despite the much lower  $\text{O}_2$

and H<sub>2</sub>O levels. This may indicate the role of hydroxyl radicals is not as critical in the total mineralization process as other researchers have suggested. It also indicates these photocatalysts will function adequately in aqueous systems containing a significant amount of miscible organic solvents.

In the case of nanosize SnO<sub>2</sub> we observed little or no size dependence of the photooxidation rate on size when comparing d=25 nm to d=58 nm SnO<sub>2</sub> colloids at the same mass concentration. Thus, it appears having larger available surface area, by itself, does not make this material more active.

*Photooxidation of PCP using nanosize MoS<sub>2</sub> and visible irradiation..* In addition to the difficulties noted above in comparing transparent solutions of nanoclusters of TiO<sub>2</sub> or SnO<sub>2</sub> to strongly multiply scattering slurry suspensions of TiO<sub>2</sub>, in the case of nanosize MoS<sub>2</sub> we also have qualitatively different absorbance characteristics between these oxide and sulfide materials. This renders direct comparison of the photooxidation kinetics of our de facto standard, Degussa P-25, to nanosize MoS<sub>2</sub> impossible. Basically, the problem is that under illumination using a 400 nm long-pass filter, TiO<sub>2</sub> has no activity, since it doesn't absorb light in the 400 nm <  $\lambda$  < 700 nm region. So, for purposes of comparison to a bulk material suspension, we chose to use a metals grade CdS bulk powder (ALFA), whose absorbance onset of 525 nm is similar to that of nanosize MoS<sub>2</sub>. However, unlike TiO<sub>2</sub>, it does exhibit some photooxidation activity using 400 nm <  $\lambda$  < 700 nm irradiation.

Figure 12 shows the relative PCP concentration vs. time for two sizes of MoS<sub>2</sub> nanoclusters compared to CdS. The concentration of each MoS<sub>2</sub> solution, as determined by XRF, is shown in the figure, and it should be noted that due to some losses during the MoS<sub>2</sub> purification/dialysis, the concentrations are less than that of the CdS slurry suspensions. All other reaction conditions were identical.

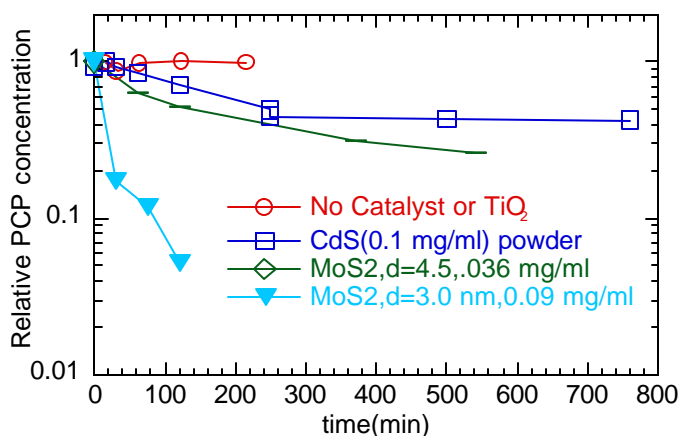


Fig. 12. Relative PCP concentration in water vs. irradiation time using a 400 W Xe arc with long and short pass filters allowing only 400 nm <  $\lambda$  < 700 nm to reach the stirred solutions.

Measurements of PCP concentration vs. irradiation time by HPLC using a 70:30 ACN:H<sub>2</sub>O to 100% ACN gradient elution allowed us to determine the concentration of the surfactant-stabilized MoS<sub>2</sub> nanoclusters while we observed the destruction of the PCP. It was necessary to use ACN

instead of MeOH as the organic component in these experiments to get good, reproducible HPLC of the nanoclusters. However, the HPLC peak symmetry of the PCP was not as good under these conditions, so we analyzed the irradiated samples using both methods. We confirmed that the MoS<sub>2</sub> nanocluster elution peak area, and corresponding optical spectrum of the nanoclusters under visible irradiation, showed no changes with irradiation time, demonstrating that the MoS<sub>2</sub> nanoclusters were acting as true photocatalysts. There seemed to be no substantial improvement in the MoS<sub>2</sub> nanocluster photooxidation kinetics when full lamp ( $300\text{ nm} < \lambda < 700\text{ nm}$ ) was used. This result is not surprising given the relatively strong visible absorbance of both sizes of MoS<sub>2</sub> nanoclusters coupled with the small lamp output below 400 nm.

Figure 12 demonstrates the dramatic effect of nanocluster size in the strong quantum confinement regime on PCP photooxidation kinetics. The change in size in this regime, it must be remembered, affects both the electronic valence and conduction band energy levels, shifting them to more favorable values with decreasing size. Adding to the complexity of a direct comparison of the size effect in MoS<sub>2</sub> to that of control catalysts, such as Degussa P25 TiO<sub>2</sub>, is the larger surface area and change in relative number of Mo edge sites with decreasing size. The key observation, never-the-less, is that both  $d=4.5$  and  $d=3.0$  nm MoS<sub>2</sub> are substantially more active than CdS, though this slurry suspension effectively absorbs a substantially larger amount of incident light than the nearly transparent (i.e. non-scattering) MoS<sub>2</sub> solutions. It should also be noted, that though we did not perform a detailed study of the effect of nanocatalyst concentration on PCP photooxidation kinetics, this effect is weak (almost linear) for nanoclusters in the 0.01 to 0.1 mg/ml range due to the low PCP concentrations used (10 ppm). Our opinion is that the dramatic differences observed in the rates of photooxidation of PCP by  $d=3.0$  MoS<sub>2</sub> at 0.09 mg/ml and  $d=4.5$  MoS<sub>2</sub> at 0.036 mg/ml, is due primarily to the wider bandgap of the former nanoclusters. This is because  $d=4.5$  nm MoS<sub>2</sub>, with an absorbance onset of nearly 600 nm, absorbs substantially more of the visible light than the  $d=3.0$  nm MoS<sub>2</sub> solution with an absorbance onset of about 450 nm. It is worth noting that the PCP photooxidation kinetics curve terminates at  $t=120$  minutes for the case of  $d=3.0$  nm MoS<sub>2</sub> simply because the next point measured at  $t=240$  minutes showed no detectable PCP (i.e., less than 20 ppb)! By way of *very indirect* comparison, this is significantly better PCP photooxidation than is achieved using Degussa P-25 TiO<sub>2</sub> and *full lamp irradiation* (i.e.,  $300\text{ nm} < \lambda < 700\text{ nm}$ )!

Another strong argument favoring the effect of energy level shifts compared to a simple increase in surface area with decreasing size on the photooxidation kinetics is our observation of nearly identical photooxidation rates for  $d=26$  nm and  $d=58$  nm SnO<sub>2</sub> nanoclusters. These SnO<sub>2</sub> sizes are much too large to affect valence and conduction band levels due to quantum confinement, yet the increase in specific surface area (total area/gram of catalyst) is very significant (almost 4x), about the same as that expected for the two sizes of much smaller MoS<sub>2</sub> nanoclusters!

We also examined our  $d=8-10$  nm MoS<sub>2</sub> nanoclusters employed in previous studies of phenol photooxidation using visible irradiation and found very little activity, showing how important the quantum confinement and concomitant energy levels shifts are on the positive results of figure 10. MoS<sub>2</sub> in the 8-10 nm size range absorbs intensely throughout the visible range  $400\text{ nm} < \lambda < 700\text{ nm}$ , but has a very small shift in the valence or conduction band levels relative to the bulk. Although its specific surface area is admittedly considerably lower, ( $\sim 10x$ ), this area reduction is not sufficient to explain its lack of activity.

**RELEVANCE, IMPACT AND TECHNOLOGY TRANSFER:**

The availability of new materials has traditionally altered technology in profound ways (e.g. carbon fiber composites, teflon, kevlar). This project successfully developed and demonstrated for the first time a new class of nanosize semi-conductors which are low cost, non-toxic, and highly effective for the complete mineralization of toxic chlorinated aromatic compounds. The impact of the engineering implementation of these new materials would be very large since the energy source, visible light from the sun, is free. The only competing technology is solid-phase carbon adsorption which, though effective and inexpensive, does leave a residual solid state toxic disposal problem. The direct formation of such benign products as CO<sub>2</sub> and HCl from the photocatalytic oxidation of chlorinated compounds by visible light is thus potentially superior. The formidable task is thus to build an efficient, flow-based, photoreactor to process large amounts of waste water. The availability and understanding of the factors influencing the activity of these new materials (e.g., size, surface treatment) makes this long range goal much more viable.

**PROJECT PRODUCTIVITY:**

A immense amount of new knowledge was gained from our investigations of novel nanosize semiconductor materials which we feel will play an increasing role in photocatalytic applications. These materials had never been considered or tried in this application prior to this work. The project was quite productive.

Personnel Supported:

J. P. Wilcoxon, T.R. Thurston (Post-doc), P. Provencio, J.E. Martin (Dept, 1122, Sandia National Labs)

D.F. Kelley, R. Parsapour (Post-doc), (Colorado State University, Dept. of Chemistry.)

**PUBLICATIONS:**

"Photocatalysis Using Nanosize Semiconductors", J.P. Wilcoxon and T.R. Thurston, Proceedings of Symposium FF, Fall MRS meeting, Boston, MA, 1998.

"Studies of Photoredox Reactions on Nanosize Semiconductors", J.P. Wilcoxon, R. Parsapour, and D.F. Kelley, , proceedings of the fourth international conference on Quantum Confinement: Nanoscale Materials, Devices, and Systems, 119th meeting of the Electrochemical Society, Montreal, Quebec, Canada, May 4-9 1997.

Peer Reviewed-

*Submitted/Accepted-*

"Photo-oxidation of Organic Chemicals Catalyzed by Nanoscale MoS<sub>2</sub>" Thurston, T.R.; Wilcoxon, J.P.; *J. Phys. Chem* **1998**, *103*, 11.

"Synthesis and Optical Properties of MoS<sub>2</sub> and Isomorphous Nanoclusters in the Quantum Confinement Regime", Wilcoxon, J.P.; Newcomer, P.; Samara, G.A.; *J. Appl. Phys.* **1997**, *81*, 7934.

"Electron Transfer Dynamics in MoS<sub>2</sub> Nanoclusters: Normal and Inverted Behavior", Parsapour, F.; Kelley, D.F.; Craft, S.; Wilcoxon, J.P.; *J. Chem. Phys.* **1996**, *104*, 1.

"Catalytic Photooxidation of Pentachlorophenol using Semiconductor Nanoclusters", J. Phys. Chem., J.P. Wilcoxon, submitted, 2000.

**INTERACTIONS:**

Presentations-

J.P. Wilcoxon, "Photooxidation of Organic Chemicals Using Semiconductor Nanoclusters", Rocky Mountain Conference on Analytical Chemistry, Denver, CO, Aug 11, 1999.

J.P. Wilcoxon, "Photocatalysis Using Semiconductor Nanoclusters, Conference on Nanocomposite Materials: Design and Applications, Anchorage, Alaska, Apr. 1999.

J.P. Wilcoxon and T.R. Thurson, "Photocatalysis Using Semiconductor Nanoclusters", MRS Meeting, Boston, MA, Dec 1998.

J.P. Wilcoxon "Applications of Metal and Semiconductor Nanoclusters as Thermal and Photo-Catalysts", 4th Intl. Conf. on Nanostructured Materials, Stockholm Sweden, June 14-19, 1998.

J.P. Wilcoxon, R. Parsapour, and D.F. Kelley, "Studies of Photoredox Reactions on Nanosize Semiconductors", Fourth International Conference on Quantum Confinement: Nanoscale Materials, Devices, and Systems, 119th meeting of the Electrochemical Society, Montreal, Quebec, Canada, May 4-9, 1997.

J.P. Wilcoxon, G.A. Samara, and P. Newcomer, "Synthesis and Optical Properties of MoS<sub>2</sub> Nanoclusters in the Strong Quantum Confinement Regime", Symposium Q, 1996 meeting of the MRS Society, Boston, MA.

J.P. Wilcoxon, F. Parsapour, and D.F. Kelley, "Studies of Photoredox Reactions on Nanosize Semiconductors", Symposium Q, 1996 meeting of the MRS Society, Boston, MA.

#### Collaborations-

D.F. Kelley-Colarado State U. (Electron Transfer Studies)

#### **PATENTS:**

J.P. Wilcoxon, "Visible light photooxidation of toxic organic chemicals using nanoscale MoS<sub>2</sub>", DOE Technical Advance/Patent Application filed Jan 1999.

#### **FUTURE WORK:**

The development of a high surface area, nanocluster impregnated photoreactor based upon a flow geometry to field test our promising results from our batch reactor studies in a more practical implementation.

#### **LITERATURE CITED.**

[1] Hoffmann, M.R.; Martin, S.T.; Choi, W.; Bahnemann, D.W.; *Chem. Rev.* **1995**, *95*, 69.

[2] Serpone, N.; Terzian, R.; Lawless, D.; Kennipohl, P.; Sauve, G.; *J. Photochem. Photobiol: A: Chem.* **1993**, *73*, 11.

[3] Mills, G.; Hoffmann, M.R.; *Environ. Sci. Technol.* **1993**, *27*, 1681.

[4] Serpone, N.; *Res. Chem. Intermed.* **1994**, *20*, 953.

[5] Thurston, T.R.; Wilcoxon, J.P.; *J. Phys. Chem* **1998**, *103*, 11.

[6] Parsapour, F.; Kelley, D.F.; Craft, S.; Wilcoxon, J.P.; *J. Chem. Phys.* **1996**, *104*, 1.

[7] Wilcoxon, J.P.; Newcomer, P.; Samara, G.A.; *J. Appl. Phys.* **1997**, *81*, 7934.